



## Research papers

## Assessment of MODIS-Aqua chlorophyll-a algorithms in coastal and shelf waters of the eastern Arabian Sea



Gavin H. Tilstone <sup>a,\*</sup>, Aneesh A. Lotikar <sup>b</sup>, Peter I. Miller <sup>a</sup>, P. Muhamed Ashraf <sup>c</sup>,  
T. Srinivasa Kumar <sup>b</sup>, T. Suresh <sup>d</sup>, B.R. Ragavan <sup>e</sup>, Harilal B. Menon <sup>f</sup>

<sup>a</sup> Plymouth Marine Laboratory, Prospect Place, West Hoe, Plymouth, PL1 3DH, UK

<sup>b</sup> Indian National Centre for Ocean Information Services (INCOIS), "Ocean Valley", P.B. No. 21, JDA Jeedimetla P.O., Hyderabad 500 055, India

<sup>c</sup> Central Institute of Fisheries Technology, Willingdon Island, Matsyapuri P.O., Cochin 682 029, India

<sup>d</sup> National Institute of Oceanography (NIO), Dona Paula 403 004, Goa, India

<sup>e</sup> Mangalore University, Mangalagangotri, Mangalore 574 199, Karnataka, India

<sup>f</sup> Goa University, Taleigao Plateau, Goa 403 206, India

## ARTICLE INFO

## Article history:

Received 17 June 2011

Received in revised form

31 January 2013

Accepted 6 June 2013

Available online 18 June 2013

## Keywords:

Case 2 waters

Coastal

Chlorophyll a

Arabian Sea

Ocean colour

MODIS-Aqua

## ABSTRACT

The use of ocean colour remote sensing to facilitate the monitoring of phytoplankton biomass in coastal waters is hampered by the high variability in absorption and scattering from substances other than phytoplankton. The eastern Arabian Sea coastal shelf is influenced by river run-off, winter convection and monsoon upwelling. Bio-optical parameters were measured along this coast from March 2009 to June 2011, to characterise the optical water type and validate three Chlorophyll-a (Chla) algorithms applied to Moderate Resolution Imaging Spectroradiometer on Aqua (MODIS-Aqua) data against *in situ* measurements. Ocean Colour 3 band ratio (OC3M), Garver-Siegel-Maritorena Model (GSM) and Generalized Inherent Optical Property (GIOP) Chla algorithms were evaluated. OC3M performed better than GSM and GIOP in all regions and overall, was within 11% of *in situ* Chla. GSM was within 24% of *in situ* Chla and GIOP on average was 55% lower. OC3M was less affected by errors in remote sensing reflectance  $R_{rs}(\lambda)$  and by spectral variations in absorption coefficient ( $a_{CDOM}(\lambda)$ ) of coloured dissolved organic material (CDOM) and total suspended matter (TSM) compared to the other algorithms. A nine year Chla time series from 2002 to 2011 was generated to assess regional differences between OC3M and GSM. This showed that in the north eastern shelf, maximum Chla occurred during the winter monsoon from December to February, where GSM consistently gave higher Chla compared to OC3M. In the south eastern shelf, maximum Chla occurred in June to July during the summer monsoon upwelling, and OC3M yielded higher Chla compared to GSM. OC3M currently provides the most accurate Chla estimates for the eastern Arabian Sea coastal waters.

Crown Copyright © 2013 Published by Elsevier Ltd. All rights reserved.

## 1. Introduction

The unprecedented coverage of ocean colour data, both spatially and temporally over the global ocean, has provided important insights into phytoplankton dynamics and biogeochemical cycling in the marine environment (Bousquet et al., 2006; Mohr and Forsberg, 2002). As a consequence, in areas such as the Arabian Sea Shelf waters, ocean colour Chlorophyll-a (Chla) data, in combination with sea surface temperature (SST) and wind speed, is being used operationally to indicate potential fishing zones and fish conservation zones (Petit et al., 2003; Royer et al., 2004).

Most operational satellite Chla algorithms are empirical, switching band ratios (O'Reilly et al., 1998, 2000). They perform well where the optically active substance in the water column is phytoplankton (Sathyendranath et al., 1999), but tend to fail in regions where the Inherent Optical Properties (IOP) are determined not only by phytoplankton, but also by absorption due to coloured dissolved organic material (CDOM) ( $a_{CDOM}(\lambda)$ ) and scattering by Total Suspended Matter (TSM) ( $b_p(\lambda)$ ) (Prieur and Sathyendranath, 1981). The presence of CDOM and TSM in coastal waters however, can cause errors in the retrieval of ocean colour Chla especially when using empirical algorithms (Darecki and Stramski, 2004). This is predicted to become worse under future climate change scenarios as TSM and CDOM become uncoupled from phytoplankton Chla (Dierssen, 2010). CDOM and TSM modify the normalised water leaving radiance ( $nL_w$ ), which can lead to significant errors in Chla retrieval from satellite (IOCCG, 2006). To overcome this problem, semi-analytical ocean colour algorithms have been developed,

\* Corresponding author. Tel.: +44 1752 633100; fax: +44 1752 633101.  
E-mail address: ghti@pml.ac.uk (G.H. Tilstone).

based on radiative transfer solutions from a knowledge of the IOP, which are usually derived from a large *in situ* database for a specific area (Lee et al., 2002; Maritorena et al., 2002; Sathyendranath et al., 2001; Tilstone et al., 2012). Parallel to the development of these algorithms, advancements in ocean colour satellite sensors, with more spectral bands and novel atmospheric correction models, has provided more accurate ocean colour products (Zibordi et al., 2006). The Moderate Resolution Imaging Spectro-radiometer onboard the Aqua satellite (MODIS-Aqua) is the current operational, medium resolution mission from NASA, and has built on previous missions, such as Sea-viewing Wide Field-of-view Sensor (SeaWiFS), by having more spectral bands and better spatial resolution. Though the accuracy of Chla algorithms for some satellite sensors in some coastal zones has been evaluated (Zibordi et al., 2009), sensor characteristics, atmospheric correction models and level 2 product algorithms used for each sensor differ (Zibordi et al., 2006). MODIS has recently experienced radiometric drift, that has been addressed through frequent vicarious calibration and re-processing of the data. The reprocessed data subsequently needs to be quantified through on-going validation exercises. An accuracy assessment of ocean products available from MODIS-Aqua is still therefore necessary and especially in coastal regions where the optical properties change more dynamically. Though ocean colour products from Coastal Zone Colour Scanner (CZCS), SeaWiFS and Indian Remote Sensing Satellite (ISR)-P4 Ocean Colour Monitor (OCM) have been validated in the open ocean waters of the Arabian Sea (Banse and English, 2000; Banzon et al., 2004; Chauhan et al., 2002; Desa et al., 2001), there have been few ocean colour validation studies in the coastal waters (Chauhan et al., 2003; Menon et al., 2006), and few for Chla products available from MODIS-Aqua (Shanmugam, 2011). There is therefore, an obvious need to assess MODIS-Aqua algorithms in coastal areas of the Arabian Sea to identify the most accurate Chla product available for the region for the on-going monitoring of phytoplankton biomass.

The principal objective of this study was to assess the performance of Chla algorithms available for MODIS-Aqua in coastal waters of the eastern Arabian Sea. The effect of potential errors in

the atmospheric correction and from CDOM and TSM were assessed. Subsequently, using the most accurate Chla algorithms, time series were generated from 2002–2011, and spatial and temporal differences between them were analysed.

## 2. Material and methods

### 2.1. Study area

The eastern Arabian Sea shelf is defined as the Western Indian Coastal Province (INDW) (Longhurst, 2007). It exhibits intense upwelling along the southern coast during the southwest (summer) monsoon, resulting in a deepening of the mixed layer and injection of subsurface nutrient rich waters to surface and enhanced biological production. During the northeast (winter) monsoon the INDW becomes oligotrophic or mesotrophic (Brock et al., 1991; Shetye et al., 1994). The area adjacent to Kochi is also influenced by the River Periyar. The northern section of the INDW above 20°N, is predominantly influenced by winter convection (Madhupratap et al., 1996) and river run-off from the Rivers Mahi, Narmada, Indus and Hab, which flow into the Gulf of Khambhat and Mouths of the Indus (the shelf region just above Area A in Fig. 1b), respectively.

A total of 326 Chla, 287 TSM and 139  $a_{CDOM}(\lambda)$  measurements were made between 22.50°N, 66.10°E and 9.90°N, 75.86°E from December 2008 to June 2011 (Fig. 1a) during six cruises aboard Ocean Research Vessel (ORV) Sagar Kanya and 48 short (1 day) cruises on fishing vessels. Of these, 50 were coincident with high quality matchups for MODIS-Aqua and within ±30 mins of the satellite overpass and were used for an accuracy assessment of MODIS-Aqua Chla algorithms (Fig. 1b). In addition, 78 *in situ* measurements of remote sensing reflectance  $R_{rs}(\lambda)$  were coincident with the MODIS-Aqua overpass and were used for evaluating the accuracy of MODIS-Aqua  $R_{rs}(\lambda)$ .

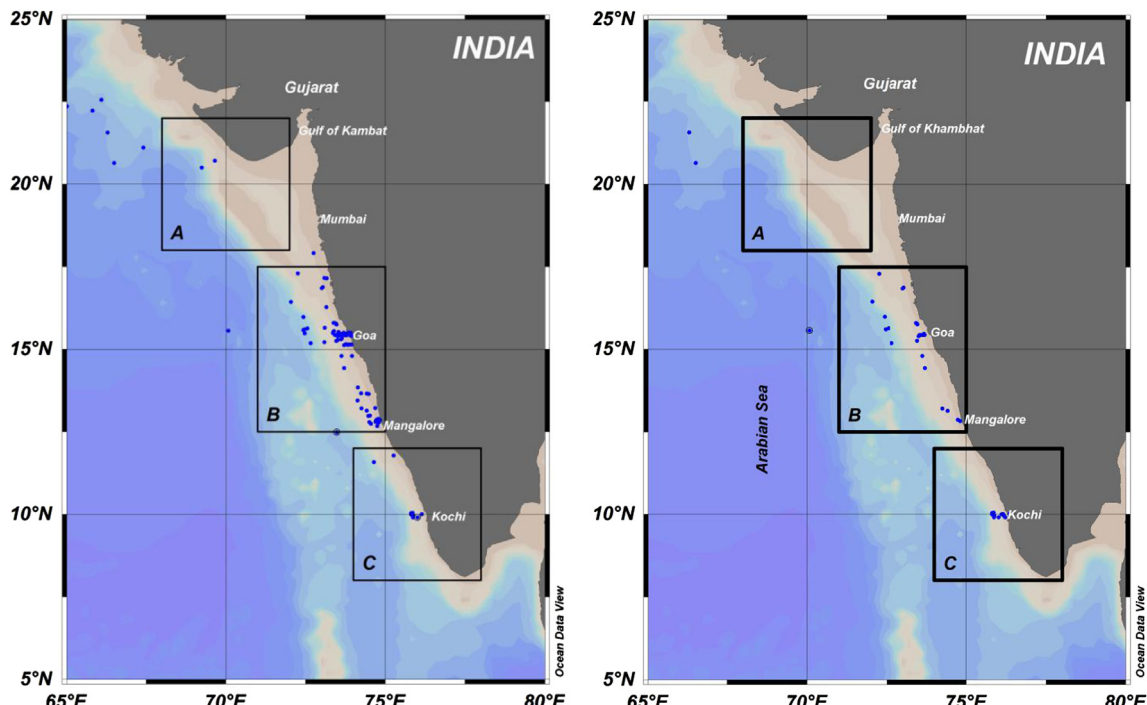


**Fig. 1.** Stations sampled along the eastern coast of the Arabian Sea for (a) all *in situ* stations sampled, (b) satellite-*in situ* Chla match-up stations. The Regions A, B and C correspond to the time series given in Fig. 7. (For interpretation of the references to colour in this figure, the reader is referred to the web version of this article.)

## 2.2. In situ remote sensing reflectance ( $R_{rs}$ )

The remote sensing reflectance ( $R_{rs}$ ) were measured hyperspectrally using Satlantic™ HyperOCR hyperspectral radiometer. The instrument has 256 optical channels between 350 nm and 800 nm that measure downwelling surface irradiance ( $E_s$ ) and profiles of downwelling irradiance ( $E_d$ ) and upwelling radiance ( $L_u$ ). The radiometers were deployed away from the vessel to avoid ship-induced perturbations and shading following the protocols of Fargion and Mueller (2000). The data were recorded using SatView™ software and processed using Prosoft™ software. When the tilt of the sensor was  $> 5^\circ$  and profiling velocity was more than  $0.7 \text{ ms}^{-1}$  the data were discarded to ensure high quality of the measurements. The majority of the observations were made at local noon and the sun and sensor viewing geometry did not change. Further technical specifications of the instruments can be found in Zibordi et al. (2011). The  $R_{rs}(\lambda)$  ( $\text{sr}^{-1}$ ) was then calculated from

$$R_{rs}(\lambda) = \frac{L_w(\lambda, 0^+)}{E_d(\lambda, 0^+)}, \quad (1)$$

where  $E_d(\lambda, 0^+)$  is the above surface downwelling spectral irradiance ( $\text{W m}^{-2} \text{ nm}^{-1}$ ) and  $L_w(\lambda)$  is the water leaving radiance ( $\text{W m}^{-2} \text{ nm}^{-1} \text{ sr}^{-1}$ ). Standard ocean optics protocols (Mueller et al., 2000) were used in the computation of water leaving radiance ( $L_w$ )

$$L_w(\lambda, 0^+) = L_u(\lambda, 0^-) \frac{[1 - \rho(\lambda, \theta)]}{\eta_w^2(\lambda)} \quad (2)$$

where  $L_u(\lambda, 0^-)$  is water leaving radiance below surface,  $\rho(\lambda, \theta)$  is Fresnel reflectance index of seawater and  $\eta_w(\lambda)$  is Fresnel refractive index of seawater.

Surface downwelling irradiance was calculated from

$$E_d(\lambda, 0^+) = \frac{E_d(\lambda, 0^-)}{(1 - \alpha)} \quad (3)$$

where  $\alpha$  is the Fresnel reflection albedo from the sun ( $\sim 0.043$ ) and  $E_d(\lambda, 0^-)$  is extrapolated from the  $E_d(\lambda, z)$  profile.

## 2.3. In situ Chla, TSM and $a_{CDOM}(\lambda)$

Chla was measured using Turner Designs™ 10 AU-field fluorometer following the Welschmeyer method (Welschmeyer, 1994). Between 0.1 L and 1 L of water were filtered onto 47 mm Glass Fibre Filters (GF/F) using a vacuum pressure of  $< 200 \text{ mm Hg}$  and extracted overnight in 90% acetone. The samples were then centrifuged for 10–20 min at 2000 rpm and the raw fluorescence

given as digital volts were converted into Chla concentrations using calibration curves from Chla standards (Sigma-Aldrich Company Ltd.). The quality of these samples was checked against Chla determined by High Performance Liquid Chromatography (HPLC) at six stations with an absolute percentage difference of 12% between HPLC and fluorometric values.

TSM was determined gravimetrically according to Strickland and Parsons (1972) and JGOFS protocols (UNESCO, 1994). In brief, the water samples were filtered through  $0.45 \mu\text{m}$  pre-weighed cellulose acetate filters (Sartorius), washed with distilled water and immediately dried in an oven at  $75^\circ\text{C}$ . They were then re-weighed in the laboratory using a Sartorius electronic balance with a detection limit  $10 \mu\text{g}$ .

$a_{CDOM}(\lambda)$  was measured spectro-photometrically following Fargion and Mueller (2000). Water samples were filtered onboard through  $0.2 \mu\text{m}$  Sartorius cellulose membrane filters. The sample transparency was measured using Shimadzu™ double beam UV-2450 spectrophotometer, over the spectral range 400–700 nm at a 1 nm resolution, in a 10 cm quartz cuvette, relative to a bi-distilled MilliQ reference blank.  $a_{CDOM}(\lambda)$  was calculated from the optical density of the sample and the cuvette path length and  $S_{CDOM}(\lambda)$  was fitted using an exponential fit from 400 nm to 700 nm following Twardowski et al. (2004). The absorption coefficients were also corrected for backscattering of small particles and colloids, which pass through filters following Green and Blough (1994).

## 2.4. Satellite data

MODIS-Aqua level-1A data, at 1 km spatial resolution, corresponding to the days of *in situ* sampling, were acquired from GSFC-NASA. The data were processed from level-1A to level-2 using SeaWiFS Data Analysis System (SeaDAS) v6.4. Chla was calculated using the following algorithms, which are freely available to end users as the standard, evaluation and test Chla products on the GSFC-NASA Ocean Colour web site: (1) OC3M, (2) GSM and (3) GIOP. The functional form of each algorithm is given in Table 1.

OC3M is a fourth-order band ratio algorithm, that uses one of two  $R_{rs}(\lambda)/R_{rs}(547)$  ratios (Table 1), depending on the reflectance characteristics of the water type (O'Reilly et al., 2000).

The GSM is an optimized semi-analytical algorithm that simultaneously retrieves Chla, absorption coefficient for dissolved and detrital materials ( $a_{dg}$ ) and the particulate backscatter coefficient ( $b_{bp}$ ) at 443 nm, from spectral measurements of  $nL_w(\lambda)$ . The parameters for the model were obtained through simulated annealing which is a global optimization technique (Maritorena et al., 2002).

**Table 1**  
Functional form of MODIS-Aqua Chla algorithms. RMS,  $r^2$ , Slope and Bias are algorithm *versus* *in situ* Chla as an indication of accuracy of each algorithm from previously published work.  
 $R = \log_{10}\{\max[(R_{rs}443/R_{rs}547), (R_{rs}448/R_{rs}547)]\}$

Algorithm	Reference	Functional form	Accuracy
OC3M	O'Reilly et al. (2000)	$\text{Chl\_a} = 10^{(a+bR+cR^2+dR^3+eR^4)}$ $R = \log_{10}\left\{\max\left[\left(\frac{R_{rs}443}{R_{rs}547}\right), \left(\frac{R_{rs}488}{R_{rs}547}\right)\right]\right\}$ $a=0.2424; b=-2.7423; c=1.8017; d=0.0015; e=-1.228$	RMS=0.255 $R^2=0.86$ Slope=1.0 Bias=0.00
GSM	Maritorena et al. (2002)	$L_w(\lambda) = \frac{tF_0(\lambda)}{n_w^2} \sum_{i=1}^2 g_i \left\{ \frac{[b_{bw}(\lambda) + b_{bp}(443)(\lambda/443)^{-1.0337}]}{[b_{bw}(\lambda) + b_{bp}(443)(\lambda/443)^{-1.0337}] + [a_w(\lambda) + \text{Chl\_a} \times a_{ph}^*(\lambda) + a_{CDOM}(443) \times e^{-0.0206(\lambda-443)}]} \right\}^i$	RMS=0.19 $R^2=0.82$ Slope=0.91 Bias=-0.021
GIOP	Franz and Werdell (2010)	$r_{rs}(\lambda, 0^-) = \frac{R_{rs}(\lambda)}{0.52 + 1.7R_{rs}(\lambda)}$ and $r_{rs}(\lambda, 0^-) = G(\lambda) \frac{b_b(\lambda)}{a_{dg}(\lambda) + b_b(\lambda)}$ $a_{ph}(\lambda) = M_{ph} \times a_{ph}^*(\lambda); a_{dg}(\lambda) = M_{dg} \times a_{dg}^*(\lambda); b_{bp}(\lambda) = M_{bp} \times b_{bp}^*(\lambda)$ $a_{dg}^*(\lambda) = e^{-0.0206(\lambda-443)}$ and $b_{bp}^*(\lambda) = \left(\frac{\lambda}{443}\right)^{-1.0337}$	RMS, $R^2$ , slope and bias not given

The GIOP model uses spectral shapes of each optically active constituent in the water column described by eigenvectors of the absorbing and backscattering components. An inversion process is performed to find the optimum set of eigenvalues between the modelled  $R_{rs}(0^-, \lambda)$  and MODIS-Aqua  $R_{rs}(0^-, \lambda)$  using the Levenburg–Marquardt optimization scheme. The GIOP model was run using the default values of Chla-normalised absorption coefficient of phytoplankton ( $a_{ph}^*$ ), TSM-normalised detrital and CDOM absorption coefficient ( $a_{dg}^*$ ), detrital and CDOM absorption coefficient slope ( $S_{dg}$ ), particle-specific backscattering coefficient ( $b_{bp}^*$ ), back-scattering coefficient slope ( $S_{bp}$ ) which are taken from the GSM model (Franz and Werdell, 2010).

## 2.5. Match-up analysis

MODIS-Aqua Chla data were extracted for a  $3 \times 3$  pixel box around the station sampled, within  $\pm 30$  mins of sampling and with no error flags raised from the following: LAND, CLDICE, NGWL, ATMWARN, ATMFAIL, CHLWARN and CHLFAIL. Boxes containing < 50% of the valid pixel data were discarded (Bailey and Werdell, 2006). A total of 50 match-ups were obtained for Chla, which were sub-divided into three coastal areas based on the ecological provinces: (1) The INDW is influenced by winter convection north of  $18^\circ\text{N}$  and based on this, Region 'A' (Fig. 1b) was defined as the area from  $18^\circ$  to  $22^\circ\text{N}$  to  $68^\circ$  to  $72^\circ\text{E}$ ; (2) South of  $12^\circ\text{N}$  INDW is affected by monsoon upwelling and Region 'C' (Fig. 1b) was defined from  $8^\circ$  to  $12^\circ\text{N}$  to  $74^\circ$  to  $78^\circ\text{E}$  to capture these hydrographic characteristics; (3) the INDW region between  $12^\circ$  and  $18^\circ\text{N}$  is a transition zone at the boundary of winter convection and monsoon upwelling, where we defined region 'B' (Fig. 1b) from  $12.5^\circ$  to  $17.5^\circ\text{N}$  to  $71^\circ$  to  $75^\circ\text{E}$ . There were too few match-ups in Region A for accuracy assessment analysis, but this region was used for comparison of satellite algorithms only in a contrasting area affected by winter convection.

To evaluate algorithm performance we used the mean ( $M$ ), standard deviation ( $S$ ) of the  $\log_{10}$ -difference error between measured and satellite Chla ( $r$ ) at each station and  $\log_{10}$  root-mean square ( $\log_{10}\text{-RMS}$ ). We also used the inverse transformed ratio between satellite and measured values  $M$  ( $F_{\text{med}}$ ),  $M-S$  ( $F_{\min}$ ) and  $M+S$  ( $F_{\max}$ ) following Campbell et al. (2002). The unbiased percentage difference (UPD) was calculated following Antoine et al. (2008) to illustrate the uncertainty between measured and satellite Chla. We employed one way analysis of variance (ANOVA) to test for significant differences between *in situ* and satellite estimates of Chla. The ANOVA results are given as  $F_{1,160}=x$  and  $P=y$  where  $F$  is the mean square to mean square error ratio, the sub-script numbers (1,160) denote the degrees of freedom and  $P$  is the ANOVA critical significance value.

## 2.6. Time-series analysis

Monthly composite of MODIS-Aqua level-3 data, with 4 km spatial resolution, from July 2002 to April 2011, were acquired from GSFC-NASA (<http://oceancolor.gsfc.nasa.gov/cgi/l3>). The spatial mean and standard derivation were computed over three grids along the eastern Arabian Sea Coast in Regions A, B and C (Fig. 1b), to compare differences against *in situ* values and between algorithms. Mean *in situ* values were computed from all values shown in Fig. 1a within each box averaged over each month sampled between 2009 and 2011. As highlighted above, there were too few data points to do this for Region A, so only differences between Chla algorithms were compared.

## 3. Results

### 3.1. Variability in Chla, TSM and $a_{CDOM}(\lambda)$

Along the central and south eastern Arabian Sea Shelf, Chla varied from  $0.01 \text{ mg m}^{-3}$  to  $38.85 \text{ mg m}^{-3}$  (Fig. 2a, b), and reached a minima during pre-monsoon and maxima during monsoon and post-monsoon. TSM varied from  $0.33 \text{ g m}^{-3}$  to  $61.27 \text{ g m}^{-3}$  (Fig. 2a, c) with maxima during the winter and pre-monsoon. The variability in

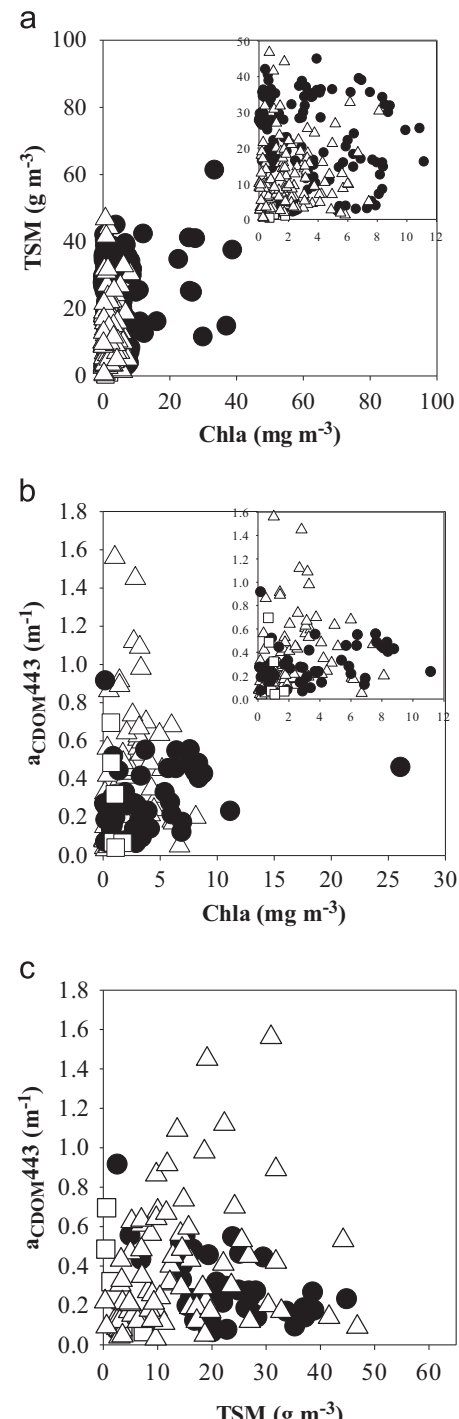


**Fig. 2.** Scatter plots showing the relationship between (a) Chla and TSM, (b)  $a_{CDOM}(443)$  and Chla and (c) TSM and  $a_{CDOM}(443)$ . Open squares are for North eastern offshore and shelf Region ('A'), closed circles are Central eastern coastal Region ('B') and open triangles are South eastern coastal Region ('C'). Insets in (a) and (b) are expanded scales.

$a_{CDOM}(443)$  was between 0.03 m<sup>-1</sup> and 1.56 m<sup>-1</sup> with maxima during the monsoon and minima during post-monsoon (Fig. 2a, b). The co-variation between Chla, TSM and  $a_{CDOM}(443)$  was assessed by linear regression. There was a significant positive co-variation between Chla and TSM ( $F_{1,284}=15.38$ ,  $P<0.0001$ ; Fig. 2a), though this only explained 5% of the variation through the following relationship:  $TSM=0.43\text{Chla}+14.93$ . The relationship between Chla and  $a_{CDOM}(443)$  was not significant ( $F_{1,138}=1.31$ ,  $P=0.254$ ; Fig. 2b), and only explained 1% of the variability between these variables. Similarly, there was no significant relationship between TSM and  $a_{CDOM}(443)$  ( $F_{1,138}=0.04$ ,  $P=0.851$ ; Fig. 2c), which explained <1% of the variance between these variables. The relationship between TSM and  $a_{CDOM}(443)$  in the South-eastern Region C was significant however ( $F_{1,47}=14.03$ ,  $P<0.0001$ ; Fig. 2c), and explained 22% of the variance between these parameters.

### 3.2. Accuracy assessment of MODIS-Aqua remote sensing reflectance

In Fig. 3, MODIS-Aqua  $R_{rs}(\lambda)$  is plotted against *in situ*  $R_{rs}(\lambda)$ . For all data there was a higher  $S$ ,  $M$ , UPD and  $\log_{10}$ -RMS for  $R_{rs}(412)$ ,  $R_{rs}(645)$  and  $R_{rs}(667)$  compared to  $R_{rs}(469)$ ,  $R_{rs}(488)$ ,  $R_{rs}(531)$  and

$R_{rs}(547)$  (Fig. 3, Table 2). The slope was 0.74 for  $R_{rs}(443)$  and 0.86 for  $R_{rs}(555)$ , but 0.54 and 0.14 for  $R_{rs}(412)$  and  $R_{rs}(645)$ , respectively. There was an under-estimation at high values of MODIS-aqua  $R_{rs}(412)$ ,  $R_{rs}(443)$  and  $R_{rs}(488)$  compared to *in situ* values resulting in high  $F_{\max}$  values, and over-estimation at lower values resulting in low  $F_{\min}$  values (Fig. 3, Table 2). This improved for  $R_{rs}(531)$ ,  $R_{rs}(547)$  and  $R_{rs}(555)$ , and the regression line was close to 1. At these wave bands however, the intercept was above 0 which resulted in a slight under-estimate of  $R_{rs}$  in the blue-green. The majority of the data were from Region B (Fig. 1b) between 13°N and 17°N and there were few data available in Region A north of 18°N. Based on the slope, intercept,  $r$ , UPD and  $\log_{10}$ -RMS,  $M$ ,  $S$  and  $F$ , the accuracy of  $R_{rs}(412)$ ,  $R_{rs}(443)$  and  $R_{rs}(645)$  was lower in Region B compared to Region C, whereas the accuracy of  $R_{rs}(469)$  to  $R_{rs}(555)$  and  $R_{rs}(667)$  was lower in Region C compared to Region B.

### 3.3. Accuracy assessment of MODIS-Aqua chlorophyll algorithms

Fig. 4 shows log-log scatter plots of *in situ* against MODIS-Aqua Chla for the OC3M, GIOP, and GSM algorithms, with the

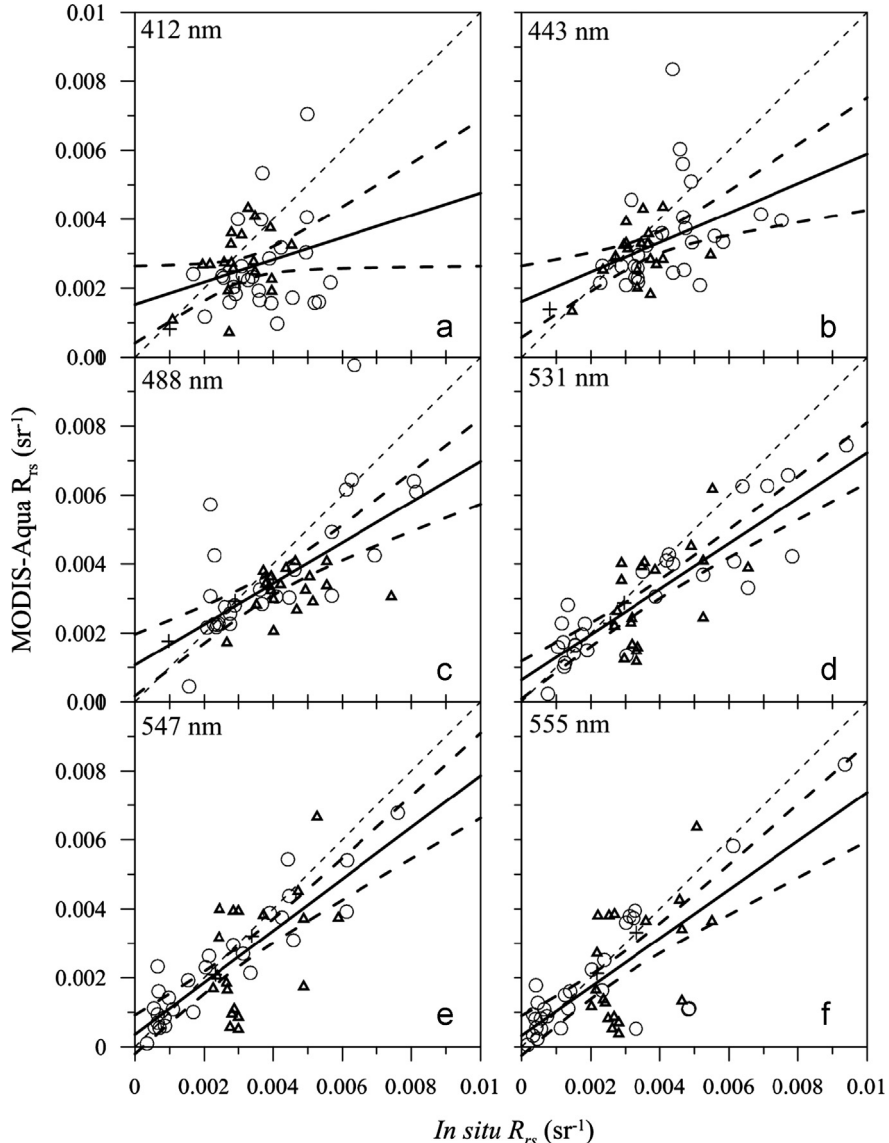


**Fig. 3.** *In situ* versus MODIS-Aqua  $R_{rs}$  for (a) 412 nm, (b) 443 nm, (c) 488 nm, (d) 531 nm, (e) 547 nm and (f) 555 nm. Symbols as in Fig. 2 except for crosses, which are for offshore north eastern region. The small dashed line is the 1:1, solid line is regression line and bold dashed lines are 95% confidence limits.

**Table 2**

Performance indices for relative errors between *in situ* and MODIS-Aqua Remote Sensing Reflectance ( $R_{rs}$ ) ( $\text{sr}^{-1}$ ). Percentage variance explained ( $R^2$ ), intercept and slope and log-difference errors in measured and satellite  $R_{rs}$  ratio ( $r$ ) as Mean ( $M$ ), Standard deviation ( $S$ ) and root-mean square ( $\text{Log}_{10}\text{-RMS}$ ). The geometric mean and one-sigma range of the ratio ( $F = \text{value}_{\text{alg}}/\text{value}_{\text{meas}}$ ) are given by  $F_{\text{med}}$ ,  $F_{\text{min}}$ , and  $F_{\text{max}}$ , respectively; values closer to 1 are more accurate. UPD is the unbiased percentage difference.

$\lambda$ (nm)	$R^2$	Slope	Intercept	$r$	UPD	$\text{Log}_{10}\text{-RMS}$	$M$	$S$	$F_{\text{med}}$	$F_{\text{max}}$	$F_{\text{min}}$
All regions	$N=78$										
412	0.11	0.54	0.001	1.55	7.32	0.25	-0.14	0.21	0.73	1.19	0.45
443	0.58	0.74	0.0001	1.27	5.44	0.29	-0.06	0.29	0.88	1.70	0.45
469	0.66	0.72	0.001	1.19	3.49	0.13	-0.06	0.12	0.87	1.14	0.66
488	0.73	0.77	0.0001	1.24	4.05	0.15	-0.07	0.14	0.85	1.16	0.62
531	0.85	0.79	0.0001	1.29	4.36	0.18	-0.08	0.16	0.83	1.20	0.57
547	0.83	0.82	0.0001	1.36	4.31	0.22	-0.08	0.20	0.83	1.32	0.52
555	0.75	0.86	0.0001	1.91	5.01	0.33	-0.11	0.32	0.78	1.62	0.38
645	0.08	0.14	0.0001	3.13	6.03	0.78	0.06	1.03	1.16	5.67	0.14
667	0.51	0.78	0.0001	1.25	4.88	6.65	0.52	1.19	3.32	9.07	0.35
Region A	$N=6$										
412	1.00	0.65	0.0	1.31	6.69	0.12	-0.12	0.05	0.76	0.84	0.69
443	0.89	0.92	0.0	1.09	1.21	0.13	-0.02	0.14	0.95	1.32	0.69
469	0.92	0.87	0	1.02	0.17	0.11	0.004	0.12	1.01	1.33	0.76
488	0.88	0.76	0.0	1.05	0.31	0.12	0.004	0.14	0.99	1.36	0.72
531	0.89	1.23	-0.001	1.21	3.91	0.12	-0.07	0.11	0.85	1.09	0.66
547	0.90	1.22	-0.001	1.28	4.66	0.15	-0.08	0.14	0.82	1.14	0.59
555	0.94	1.23	-0.001	1.26	4.39	0.15	-0.08	0.14	0.83	1.15	0.60
645	0.12	0.19	0.00	1.47	9.60	0.33	-0.19	0.30	0.65	1.30	0.33
667	0.08	-0.06	0.0	1.96	9.6	0.36	-0.19	0.38	0.65	1.55	0.27
Region B	$N=58$										
412	0.10	0.59	0.001	1.68	9.19	0.28	-0.17	0.22	0.67	1.13	0.40
443	0.58	0.76	0.0	1.31	6.25	0.33	-0.06	0.32	0.87	1.87	0.41
469	0.68	0.72	0.001	1.16	2.85	0.13	-0.05	0.12	0.89	1.17	0.68
488	0.76	0.79	0.001	1.21	3.31	0.15	-0.06	0.14	0.87	1.20	0.64
531	0.89	0.79	0.0	1.25	3.61	0.17	-0.05	0.16	0.86	1.23	0.59
547	0.91	0.81	0.0	1.22	2.95	0.18	-0.05	0.17	0.89	1.33	0.59
555	0.82	0.87	0.0	1.90	3.57	0.33	-0.08	0.32	0.83	1.75	0.39
645	0.11	0.14	0.0	3.66	8.86	0.88	-0.06	0.89	0.86	6.79	0.11
667	0.85	0.79	0.0	1.19	4.32	0.71	0.20	0.69	1.60	7.85	0.33
Region C	$N=14$										
412	0.06	0.31	0.002	1.31	3.66	0.20	-0.07	0.19	0.85	1.33	0.54
443	0.02	0.15	0.002	1.22	3.98	0.14	-0.07	0.12	0.85	1.13	0.64
469	0.03	0.13	0.003	1.40	7.48	0.17	-0.13	0.10	0.74	0.93	0.58
488	0.02	0.08	0.003	1.45	8.41	0.18	-0.15	0.10	0.71	0.89	0.56
531	0.29	0.67	0.0	1.49	7.47	0.22	-0.14	0.18	0.73	1.11	0.48
547	0.28	0.82	0.0	1.91	9.41	0.37	-0.18	0.29	0.65	1.27	0.33
555	0.28	0.83	0.0	2.17	10.81	0.38	-0.22	0.33	0.61	1.29	0.28
645	0.46	1.79	0.0	1.91	4.84	0.53	0.08	0.54	1.20	4.19	0.35
667	0.36	2.10	0.0	1.26	9.05	0.54	0.19	0.52	1.57	5.24	0.47

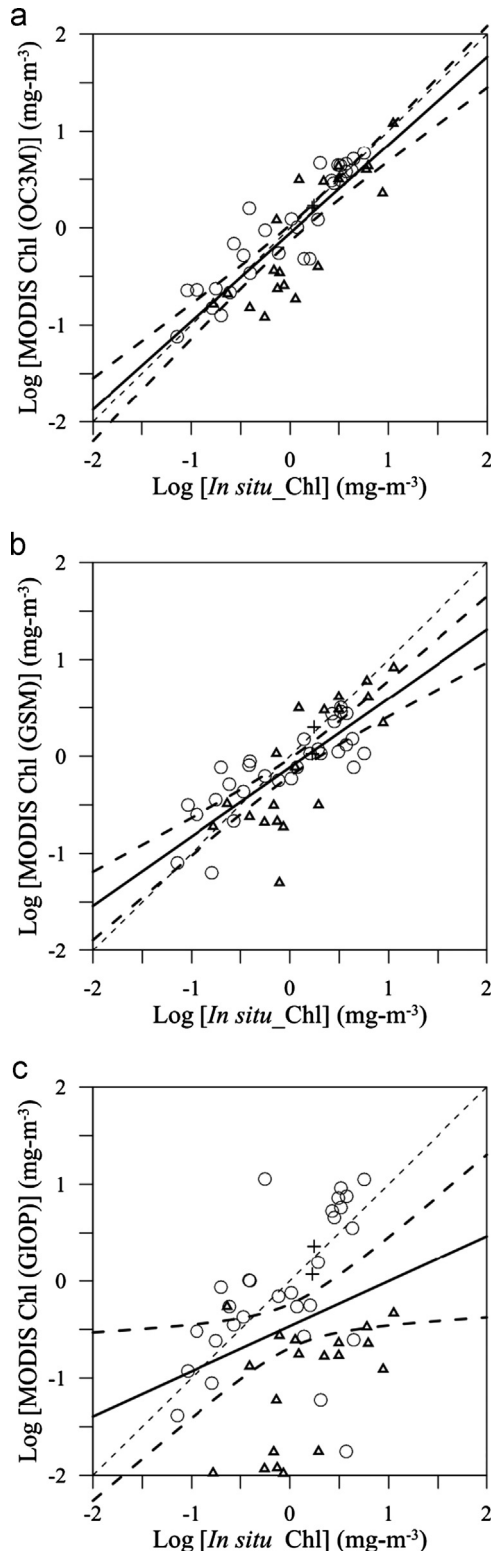


**Fig. 4.** Log–log plots of *in situ* versus MODIS-Aqua Chl for (a) OC3M, (b) GSM, and (c) GIOP algorithm. Symbols and lines as in Fig. 3.

corresponding validation statistics given in Table 3. OC3M had the lowest  $\log_{10}$ -RMS, UPD,  $M$ ,  $S$  and intercept and slope,  $F_{\text{med}}$  and  $F_{\text{min}}$  closest to 1. There was no significant difference between *in situ* Chla and OC3M ( $F_{1,99}=0.25$ ,  $P=0.620$ ) and GSM ( $F_{1,99}=1.36$ ,  $P=0.247$ ). GSM  $r$  and  $F_{\text{max}}$  were closest to 1 (Table 3). GIOP was the least accurate of the algorithms, had the lowest percentage variance explained, slope, log difference,  $F_{\text{min}}$ ,  $F_{\text{med}}$ , and  $F_{\text{max}}$  and

the highest intercept,  $\log_{10}$ -RMS, UPD,  $M$  and  $S$  (Table 3). GIOP consistently under-estimated Chla (Fig. 4c, Table 3), which resulted in a significant difference between *in situ* and GIOP Chla ( $F_{1,99}=11.44$ ,  $P>0.001$ ).

On a regional basis, the trend in Region B was the same for the whole dataset, with OC3M having the lowest  $\log_{10}$ -RMS, UPD,  $M$ ,  $S$  and intercept and GSM having a similar  $r$  and  $F_{\text{max}}$ . Retrieval accuracy of OC3M, GSM and GIOP was better in Region B compared to the other Regions (Table 3). Based on the 11 statistical parameters computed, OC3M was still the most accurate algorithm in Region C, however the performance of GSM improved, having an equally accurate  $r^2$ ,  $r$ , UPD,  $M$ ,  $F_{\text{med}}$  and  $F_{\text{max}}$  closer to 1 compared to OC3M. For GIOP in the south-east Region C, there was a consistent under-estimate of Chla between  $0.07 \text{ mg m}^{-3}$  and  $11.2 \text{ mg m}^{-3}$ , whereas in Region B the accuracy of GIOP was greatly improved. There were too few match-up data for a comprehensive validation of MODIS-Aqua Chla algorithms in Region A. These results indicate that of the MODIS-Aqua algorithms tested in coastal waters of eastern Arabian Sea, OC3M is the most accurate, but south of  $12^\circ\text{N}$  adjacent to Kochi, OC3M and GSM showed a similar accuracy.

The spatial variability between OC3M, GSM and GIOP algorithms as composite maps for January, April and October 2005, representative of winter, pre and post-monsoon, was also assessed (Fig. 5). The Monsoon period (June–August) was not considered due to poor satellite coverage. All algorithms showed the same spatial and temporal patterns with high Chla offshore in the northern Arabian Sea during January and lower values in April 2005. Chla then increased again during October 2005, but became confined to the northern sector. In the offshore region of the southern Arabian Sea, Chla values were low ( $<0.1 \text{ mg m}^{-3}$ ) in January, whereas during April 2005 two prominent filaments occurred ( $\sim 0.5 \text{ mg m}^{-3}$ ) meandering from the coast to off-shore at  $15^\circ\text{N}$ ,  $75^\circ\text{E}$  and  $9^\circ\text{N}$ ,  $76.5^\circ\text{E}$ . Chla increased  $>1 \text{ mg m}^{-3}$  throughout the southern Arabian Sea during October 2005. Along the eastern Arabian Sea coast, Chla values were high ( $1\text{--}5 \text{ mg m}^{-3}$ ) in January and October and lower ( $<1 \text{ mg m}^{-3}$ ) during April 2005. During October 2005, high Chla values extended further from the coast to the shelf especially off south-east India.

The magnitude of the Chla differed between algorithms. Consistently in all months, OC3M gave the highest Chla along the entire eastern Arabian Sea coast, except in the Gulf of Khumbhat, where GSM showed the highest values, which were  $>20 \text{ mg m}^{-3}$ . For OC3M Chla values along the coast during January 2005 were between  $5 \text{ mg m}^{-3}$  and  $10 \text{ mg m}^{-3}$ ,  $0.5\text{--}5 \text{ mg m}^{-3}$  during April 2005 and increased to between  $5 \text{ mg m}^{-3}$  and  $30 \text{ mg m}^{-3}$  during October 2005. By comparison, GSM had a lower range during all months and were  $0.5\text{--}5 \text{ mg m}^{-3}$  during April and January 2005, and  $1\text{--}7 \text{ mg m}^{-3}$  in October 2005 (Fig. 5). GIOP exhibited the lowest Chla values during all months between  $0.05 \text{ mg m}^{-3}$  and  $1 \text{ mg m}^{-3}$  in January,  $0.05$  and  $0.5 \text{ mg m}^{-3}$  in April and  $0.5$  and  $2 \text{ mg m}^{-3}$  in October 2005. Both GSM and GIOP returned a large number of drop-out pixels in January and October close to the coast, especially around the Gulf of Khumbhat. Based on the statistical parameters, given in Table 3, in the subsequent satellite time series analyses we used OC3M and GSM algorithms to assess the differences between them.

### 3.4. Spatial and temporal variation in Chla algorithms available for MODIS-Aqua

In Fig. 6 we present a nine year time series of Chla from July 2002 to April 2011 for both OC3M and GSM in three coastal regions and overlay the *in situ* Chla data. In the north-eastern coastal area ('Region A'; Fig. 6a) the maximum Chla was from December to February and lower values occurred during the

**Table 3**

Performance indices for relative errors between *in situ* measured and MODISA derived Chla for OC3M, GSM, GIOP and OC5. Percentage variance explained ( $r^2$ ), intercept and slope and log-difference errors in measured and satellite Chla ratio ( $r$ ) as Mean ( $M$ ), Standard deviation ( $S$ ) and root-mean square ( $\text{Log}_{10}\text{-RMS}$ ). The geometric mean and one-sigma range of the ratio ( $F = \text{value}_{\text{alg}}/\text{value}_{\text{meas}}$ ) are given by  $F_{\text{med}}$ ,  $F_{\text{min}}$ , and  $F_{\text{max}}$ , respectively; values closer to 1 are more accurate. UPD is the unbiased percentage difference. The algorithm with the highest Chla precision is highlighted in bold.

	$r^2$	Slope	Intercept	$r$	UPD	$\text{Log}_{10}\text{-RMS}$	$M$	$S$	$F_{\text{med}}$	$F_{\text{max}}$	$F_{\text{min}}$
All regions	<b><math>N=50</math></b>										
OC3M	<b>0.73</b>	<b>0.83</b>	<b>0.261</b>	<b>1.09</b>	<b>10.74</b>	<b>0.309</b>	<b>-0.057</b>	<b>0.307</b>	<b>0.877</b>	<b>1.778</b>	<b>0.433</b>
GSM	0.61	0.55	0.313	<b>1.02</b>	23.56	0.381	-0.124	0.363	0.751	<b>1.734</b>	0.325
GIOP	0.04	0.26	1.102	1.32	56.37	0.977	-0.483	0.858	0.329	2.368	0.046
Region A	<b><math>N=2</math></b>										
OC3M	nd	nd	nd	<b>0.949</b>	<b>5.19</b>	<b>0.023</b>	<b>-0.023</b>	<b>0.004</b>	nd	nd	nd
GSM	nd	nd	nd	0.876	17.11	0.150	-0.076	0.182	nd	nd	nd
GIOP	nd	nd	nd	<b>0.996</b>	<b>5.23</b>	0.140	<b>-0.023</b>	0.196	nd	nd	nd
Region B	<b><math>N=29</math></b>										
OC3M	<b>0.86</b>	<b>1.074</b>	<b>0.086</b>	<b>1.300</b>	10.83	<b>0.241</b>	<b>0.050</b>	<b>0.240</b>	<b>1.121</b>	<b>1.951</b>	<b>0.645</b>
GSM	0.40	0.341	0.505	<b>1.152</b>	12.79	0.342	-0.064	0.342	0.864	<b>1.897</b>	0.393
GIOP	0.31	1.212	0.511	2.067	<b>5.67</b>	0.691	<b>-0.045</b>	0.702	<b>0.901</b>	4.534	0.179
Region C	<b><math>N=19</math></b>										
OC3M	<b>0.69</b>	<b>0.768</b>	<b>0.076</b>	<b>0.795</b>	<b>44.25</b>	<b>0.898</b>	<b>-0.223</b>	<b>0.344</b>	<b>0.598</b>	1.321	<b>0.271</b>
GSM	<b>0.68</b>	0.614	0.371	<b>0.828</b>	<b>40.67</b>	2.000	<b>-0.222</b>	0.399	<b>0.600</b>	<b>1.505</b>	0.239
GIOP	0.18	0.021	0.114	0.209	156.46	1.162	1.200	0.599	0.063	0.251	0.016

monsoon months from July and August. In this region, GSM consistently gave higher Chla ( $0.14\text{--}12.75\text{ mg m}^{-3}$ ) compared to OC3M ( $0.24\text{--}4.60\text{ mg m}^{-3}$ ), especially during the winter in all years except 2008 and 2010. OC3M Chla however, was closest to the *in situ* data, though these were few (Fig. 6a). In Region 'B', both algorithms indicated the maximum Chla in June (Fig. 6b), with the highest in 2005. OC3M yielded slightly higher Chla ( $0.18\text{--}2.76\text{ mg m}^{-3}$ ) compared to GSM ( $0.08\text{--}1.98\text{ mg m}^{-3}$ ), but in January 2007 and July 2010 GSM > OC3M. Again OC3M was closest to the *in situ* Chla values, but for both algorithms there was a consistent under-estimate in Chla compared to the *in situ* values. In area 'C' on the south-east coast, both algorithms showed the same temporal pattern, with low Chla values during the winter months and high values during the monsoon months (Fig. 6c). There was a good correlation between *in situ* Chla and the two algorithms (Table 3), though slightly better for OC3M, which consistently gave higher values ( $0.16\text{--}12.71\text{ mg m}^{-3}$ ) than GSM ( $0.11\text{--}7.66\text{ mg m}^{-3}$ ) especially during the monsoon and in 2002, 2003, 2004, 2007 and 2008. Of the three areas studied on the eastern Arabian Sea coast, the south-east coast had the highest Chla and the central region had the lowest values (Fig. 6b, c).

The differences between OC3M and GSM were further analysed using monthly composites of October from 2002–2010 and presented as a difference maps for each year (Fig. 7). There was no difference between OC3M and GSM in the offshore waters south of  $16^\circ\text{N}$ , where Chla was between  $0.01\text{ mg m}^{-3}$  and  $0.5\text{ mg m}^{-3}$ . Along the coastal area south of  $16^\circ\text{N}$ , OC3M gave higher Chla except in 2010 when GSM gave higher values. North of  $16^\circ\text{N}$  GSM consistently yielded higher Chla values (Fig. 7).

## 4. Discussion

### 4.1. Bio-optical properties of the eastern Arabian Sea coast

There was a significant correlation between Chla and TSM (Fig. 2a), suggesting that either (1) at the time of the monsoon blooms, inorganic TSM is also input to the sea surface through re-suspension from the sea floor or river run-off, (2) or that the monsoon blooms result in high organic TSM that co-varies with phytoplankton Chla, (3) or both of these processes occur. There was no significant correlation between Chla and  $a_{\text{CDOM}}(443)$ , suggesting that in these coastal waters  $a_{\text{CDOM}}(443)$  is de-coupled

from phytoplankton biomass, indicating that CDOM is predominantly from riverine sources. During the late winter monsoon along the north eastern Arabian Sea coast,  $a_{\text{CDOM}}(443)$  can be higher than the values we measured. We only obtained eight samples during February in shelf and off-shore waters North of  $18^\circ\text{N}$ . Menon et al. (2006) showed that  $a_{\text{CDOM}}(440)$  varied from  $5.0\text{ m}^{-1}$  to  $11.5\text{ m}^{-1}$  along this region of the coast can vary from  $0.92\text{ m}^{-1}$  to  $2.07\text{ m}^{-1}$  during the late winter monsoon in January 2003 in the shelf and offshore waters of the northern Arabian Sea between  $16^\circ\text{N}$  and  $24^\circ\text{N}$ . Similar to Menon et al. (2006), we found that Chla and TSM were highest in the coastal waters north of  $18^\circ\text{N}$ . We also observed that  $a_{\text{CDOM}}(443)$  was also high in Region B between  $12^\circ\text{N}$  and  $18^\circ\text{N}$ . From the *in situ* data, and using the optical classification Prieur and Sathyendranath (1981), Region C is Chla-TSM- $a_{\text{CDOM}}$  type coastal waters with high concentrations of these three variables, Region B is TSM- $a_{\text{CDOM}}$  type waters and Region A is Chla-TSM- $a_{\text{CDOM}}$  type coastal waters with lower concentrations of these variables. During the late winter, Region A however, may become dominated by  $a_{\text{CDOM}}$  alone (Menon et al., 2006).

### 4.2. Validation of MODIS-Aqua Chla algorithms

To assess the performance of the MODIS-Aqua Chla algorithms in coastal waters, we firstly addressed the question; what is the accuracy of MODIS-Aqua  $R_{\text{rs}}(\lambda)$ ? As outlined in the results Section 3.2 (Fig. 3, Table 2), compared to *in situ*  $R_{\text{rs}}(\lambda)$ , MODIS-Aqua  $R_{\text{rs}}(\lambda)$  was more accurate at  $R_{\text{rs}}(547)$  and  $R_{\text{rs}}(488)$  than it was at  $R_{\text{rs}}(443)$  and the retrieval accuracy of  $R_{\text{rs}}(412)$  was poor. This indicates possible errors in the atmospheric correction affecting the blue bands. For  $R_{\text{rs}}(443)$ , though there were more data available in Region C, the scatter around the 1:1 line was similar for Regions B and C. Due to the tendency of MODIS-Aqua to over-estimate  $R_{\text{rs}}(443)$  at low values (i.e. when Chla is high), the use of the  $R_{\text{rs}}(443):R_{\text{rs}}(547)$  ratio would result in a lower than expected ratio and therefore lower Chla values, which was particularly evident in Region C (Fig. 4a). The GSM algorithm uses  $R_{\text{rs}}(443)$  to partition the absorption coefficient of CDOM+detrital material ( $a_{\text{dg}}(443)$ ) and the particle-specific backscattering coefficient ( $b_{\text{bp}}(443)$ ). It then uses a simulated annealing procedure to retrieve  $a_{\text{ph}}^{*}(\lambda)$  at 412, 443, 488, 530 and 555 nm and from this calculates Chla. Since MODIS-Aqua over-estimates  $R_{\text{rs}}(443)$  at low values and under-estimates  $R_{\text{rs}}(443)$  at high values, this error will propagate into the

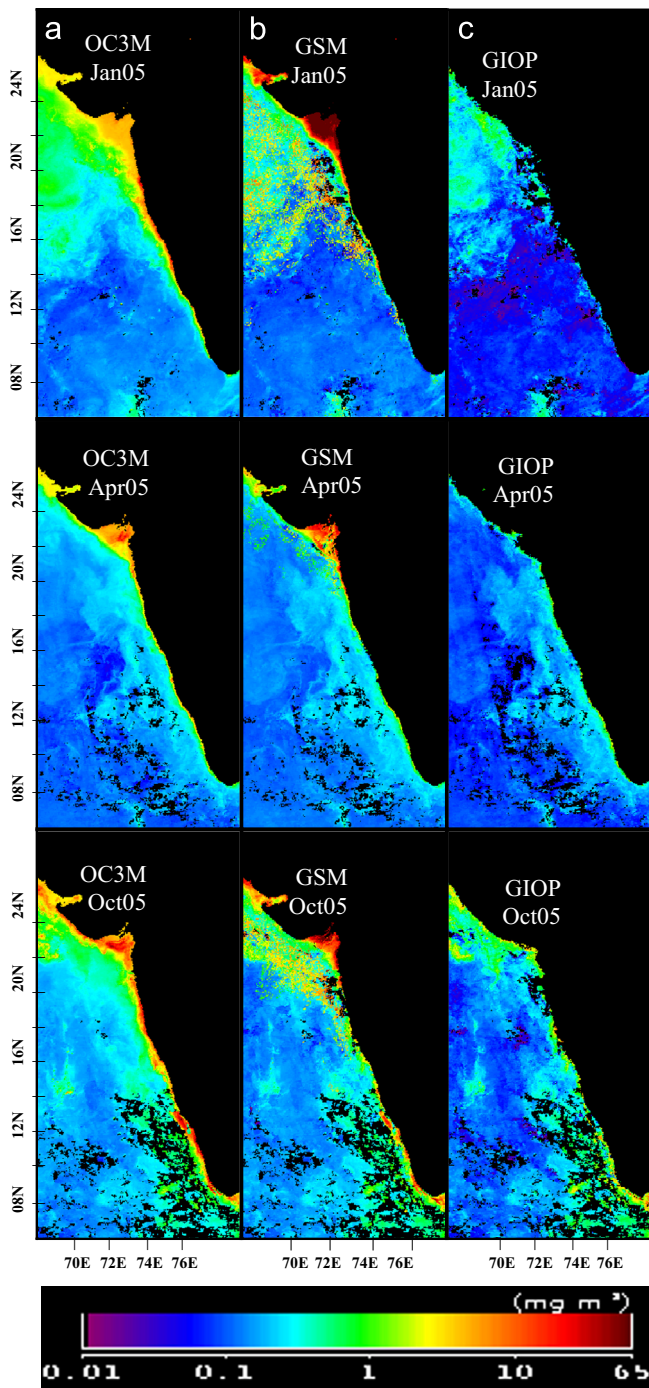


**Fig. 5.** Mean monthly composite of Chla derived from MODIS-Aqua, using (a) OC3M, (b) GSM, (c) GIOP, for January 2005 (top panel), April 2005 (middle panel) and October 2005 (bottom panel).

partitioning of  $a_{dg}(443)$  and  $b_{bp}(443)$ , the estimation of  $a_{ph}^*(443)$  and hence Chla. Of the 50 satellite-*in situ* Chla match-ups obtained, for OC3M 33 of these used the  $R_{rs}(488):R_{rs}(547)$  ratio. Thus due to greater errors in  $R_{rs}(443)$  compared to  $R_{rs}(488)$  possibly arising from errors in the atmospheric correction, the accuracy of GSM was lower than OC3M. The GIOP algorithm using the default parameters was the least accurate algorithm. The low MODIS-Aqua  $R_{rs}(\lambda)$  highlighted in Fig. 3, probably caused the inversion technique to fail to find a realistic solution for GIOP to model  $R_{rs}(\lambda)$ .

We also addressed the question; what is the effect of  $a_{CDOM}(443)$  and TSM on the Chla algorithms? To assess the effect

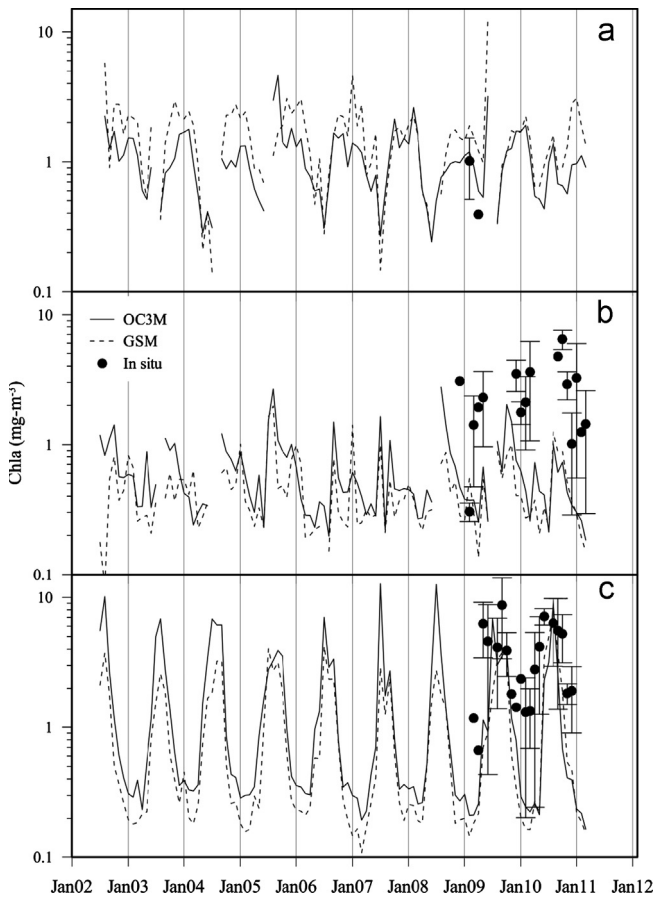


**Fig. 6.** Mean monthly Chla time series generated from MODIS-Aqua for coastal region (a) 18–22°N and 68–72°E, (b) 12.5–17.5°N and 71–75°E and (c) 8–12°N and 74–78°E. Solid line is for OC3M; dotted line is GSM. The filled circles are mean monthly *in situ* Chla and the vertical bars are the standard deviation.

of TSM and  $a_{CDOM}(443)$  on the Chla algorithms, in Fig. 8 we plot the MODIS-Aqua Chla:*in situ* Chla ratio against *in situ* TSM and  $a_{CDOM}(443)$ . A significant correlation with TSM or  $a_{CDOM}(443)$  would suggest that the error in MODIS-Aqua Chla could be partially accounted for by either of these variables. For OC3M and GSM there was no significant correlation between MODIS-Aqua Chla:*in situ* Chla ratio and  $a_{CDOM}(443)$  (Fig. 8a, b). Due to the exponential shape of  $a_{CDOM}(\lambda)$ , for the MODIS-Aqua bands,  $R_{rs}(412)$  is the band most affected by  $a_{CDOM}$ . Since OC3M band ratio principally uses  $R_{rs}(488)$  and  $R_{rs}(447)$ , it is less susceptible to errors due to high  $a_{CDOM}$ , which partially explains why it was the most accurate of the algorithms tested. For GIOP there was a significant correlation between GIOP Chla:*in situ* Chla ratio and  $a_{CDOM}(443)$  ( $F_{1,49}=4.90$ ,  $P=0.042$ ), which accounted for 23% of the variance in the error of the algorithm (Fig. 8c). This suggests that part of the error in GIOP also occurs in the partitioning between  $a_{ph}(\lambda)$  (as a proxy for Chla) and  $a_{CDOM}(\lambda)$ . The percentage variance explained was principally due to the variability MODIS-Aqua Chla:*in situ* Chla ratio and  $a_{CDOM}(443)$  in Region C, suggesting a high error in partitioning  $a_{ph}(\lambda)$  and  $a_{CDOM}(\lambda)$  for GIOP in this region, which has comparatively high CDOM-TSM-Chla (Fig. 2). For all three algorithms, there was no significant regression between MODIS-Aqua Chla:*in situ* Chla ratio and TSM (Fig. 8d–f), illustrating that for eastern Arabian Sea coastal waters, TSM has little effect on MODIS-Aqua Chla. This contrasts coastal waters of the neighbouring Bay of Bengal where TSM concentrations can be ~5 times higher and can affect the performance of some Chla algorithms available for SeaWiFS (Tilstone et al., 2011).

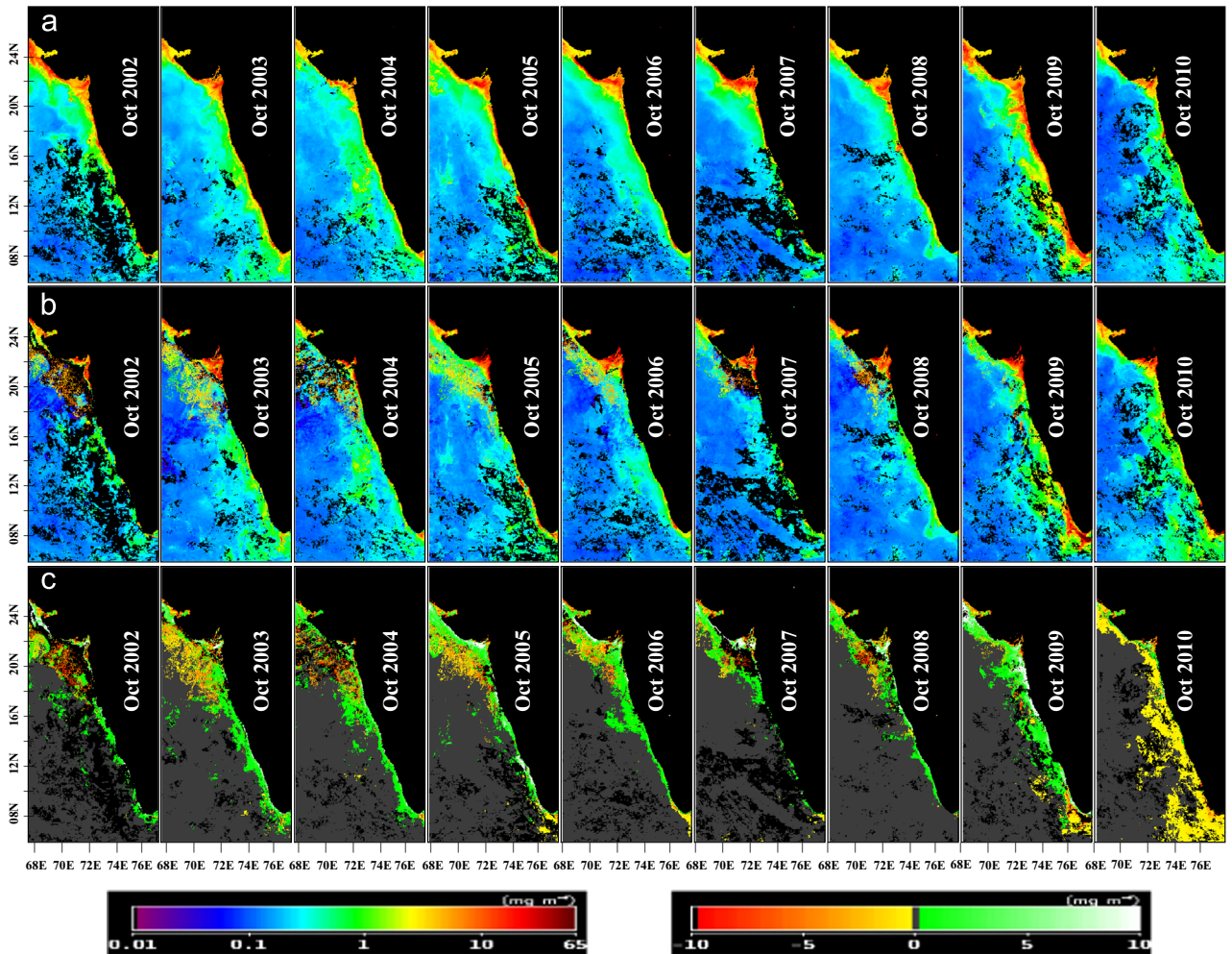


**Fig. 7.** MODIS-Aqua Chla composite for the month of October 2002–2010 for (a) OC3M algorithm, (b) GSM algorithm and (c) difference maps between OC3M and GSM algorithm. Left colour scale is for (a) and (b). Right colour scale is for (c), where red-yellow colour indicates GSM > OC3M, green indicates OC3M > GSM and grey indicates OC3M=GSM. (For interpretation of the references to colour in this figure legend, the reader is referred to the web version of this article.)

To assess whether the error in the Chla algorithms is due to bottom reflectance, we also plot the MODIS-Aqua Chla:*in situ* Chla ratio against depth. Both OC3M and GIOP show no significant correlation between MODIS-Aqua Chla:*in situ* Chla ratio and depth (Fig. 8g, i). The ratio between GSM Chla:*in situ* Chla and depth is significant ( $F_{1,47}=14.59$ ,  $P < 0.00001$ ) and explained 23% of the variance in the error (Fig. 8h), but the algorithm tended to overestimate Chla at depths  $> 200$  m, principally in area B. This suggests that the error in the algorithm is greater where the water column is deeper, suggesting that bottom reflectance does not adversely affect the algorithms tested in these shelf waters.

In summary, of the three MODIS-Aqua algorithms tested for coastal waters of the eastern Arabian Sea Shelf, OC3M was the most accurate Chla algorithm. This is principally because it uses the  $R_{rs}(488):R_{rs}(547)$  ratio which is less affected by atmospheric correction errors in the blue and high  $a_{CDOM}(\lambda)$ . Similarly, for IRS-P4 OCM in these waters Chauhan et al. (2002) found a high correlation ( $R^2=0.9$ ) between *in situ* and IRS-P4 OCM OC2 Chla. Desa et al. (2001) also showed that  $R_{rs}(490):R_{rs}(555)$  ratio is a better indicator of Chla in eastern Arabian Sea. They illustrated this by modifying SeaWiFS OC4v4 coefficients for these waters, resulting in further improvements in the  $R^2$  (0.93), slope (0.96) and S (0.26) for Chla retrieval. Shanmugam (2011) however, suggested that although OC3 reliably estimates Chla in open ocean waters, it tends to over-estimate Chla in the coastal waters of the Arabian Sea. For such optically complex waters, he developed an Algal

Bloom Index (ABI) algorithm based on a power law for the band ratios  $R_{rs}(490):R_{rs}(555)$ , which produces lower Chla values than OC3M for the Arabian Coastal zone. In his study, using the NOMAD *in situ* data base, OC3 however had a smaller mean relative error, RMSE and intercept than the ABI. Though the other validation data sets he used were large, the number of validation data points in the Arabian Sea coastal zone was small compared to this study.

The GSM algorithm is semi-analytical in function and initial IOP parameters were taken from the SeaBAM dataset and tuned by simulated annealing (Maritorena et al., 2002). It solves  $a_{ph}(\lambda)$  in the presence of TSM and  $a_{CDOM}(\lambda)$  by using a constant  $S_{CDOM}$  of  $0.0206 \text{ m}^{-1} \text{ nm}^{-1}$ , a power-law exponent for particulate backscattering ( $\eta=1.03373$ ) expressed as a function of Chla (Morel and Maritorena, 2001) and an optimized  $a_{ph}^*(\lambda)$  [ $a_{ph}^*(443)=0.05582$ ]. By comparison, we found along the south-eastern Arabian Sea coast, that the mean  $S_{CDOM}$  was  $0.0123 \text{ m}^{-1} \text{ nm}^{-1}$  and therefore lower than that used in the GSM, which may partially account for the differences between *in situ* and GSM Chla. We have no  $a_{ph}^*(\lambda)$ ,  $a_{dg}(443)$  and  $b_{bp}(\lambda)$  to compare against the values used in the global GSM parameterisation.

The GIOP and GSM algorithms are similar in that they both use shape functions to describe the absorbing and backscattering components with an analytical bb/a formulation. Using the default MODIS-Aqua parameters adopted from the GSM model, GIOP was however the least accurate algorithm. The GIOP differs from GSM in that it uses  $R_{rs}(\lambda, 0^-)$  rather than  $nL_w$  and it implements

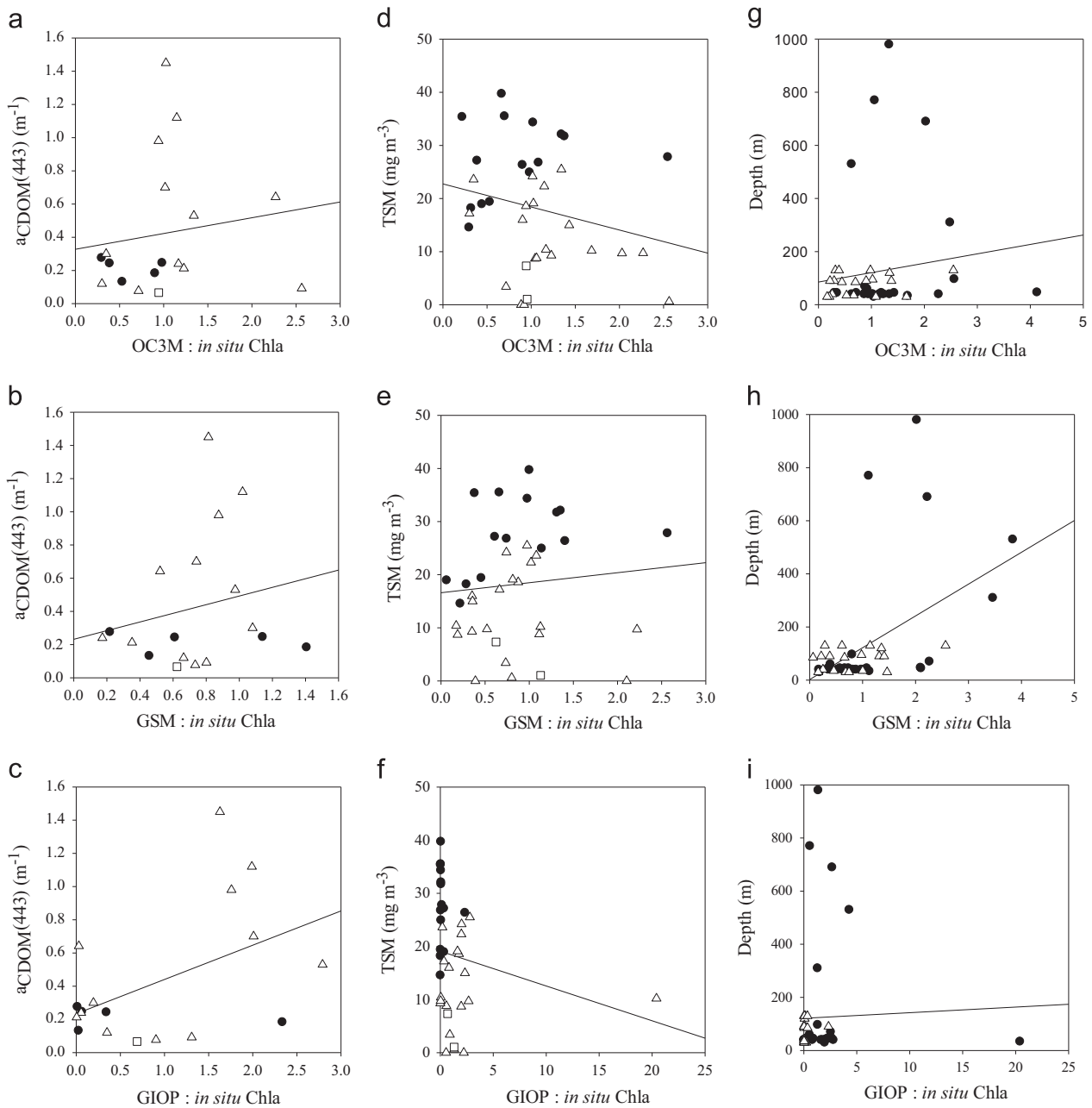


**Fig. 8.** Ratio of MODIS-Aqua Chla:in situ Chla versus  $a_{CDOM}(443)$  for (a) OC3M, (b) GSM, (c) GIOP, and versus TSM for (d) OC3M, (e) GSM, (f) GIOP, and versus depth for (g) OC3M, (h) GSM, (i) GIOP. Symbols as in Fig. 2.

empirical methods to convert  $R_{rs}(\lambda, 0^+)$  to  $R_{rs}(\lambda, 0^-)$ . It then defines specific spectral shapes for sIOP and inverts them to generate  $R_{rs}(\lambda, 0^-)$  and outputs an optimum set of eigen values (Table 1), that minimize the difference between the modelled and measured  $R_{rs}(\lambda, 0^-)$ . As highlighted above, part of the error in GIOP Chla is from MODIS-Aqua  $R_{rs}(412)$  and  $R_{rs}(443)$  due to failure in the atmospheric correction. This will lead to errors in propagating  $R_{rs}(\lambda, 0^-)$  to the respective sIOP. Part of the error using the default settings may also arise from the segregation between  $a_{ph}^*(\lambda)$  to Chla and  $a_{CDOM}(\lambda)$  (Fig. 8c). To improve the GIOP a regional parameterization is suggested (Franz and Werdell, 2010), however we did not have sufficient data on the specific-absorption, backscattering and scattering properties of phytoplankton and TSM, to do this. As highlighted by Franz and Werdell (2010), if the eigenvectors are not spectrally unique, the optimization of the eigenvalues will be highly correlated, the uncertainties could be large, and the model may not converge. Using the GIOP model

with the default parameters for the eastern Arabian Sea coast, this is evidently the case. The GIOP model is designed as a test platform for algorithm development. An initial default configuration for GIOP was defined (Franz and Werdell, 2010), which includes a fixed spectral slope for  $a_{dg}(443)$  of 0.018, an assigned specific phytoplankton absorption coefficient following Bricaud et al. (1995), an assigned spectral backscattering dependency following the QAA and Levenburg–Marquardt optimisation. Evidently, this parameterisation is not optimal for the coastal waters of the Arabian Sea. Further absorption and backscattering data is required from this region to improve the parameterisation of the GIOP and for the development of future semi-analytical algorithms for this region.

We conclude that OC3M was within 11% of in situ Chla and compared to GSM and GIOP, is the most accurate MODIS-Aqua Chla algorithm for coastal regions of the eastern Arabian Sea. GSM also proved to be accurate for these waters and was within 24% of

*in situ* Chla. Further characterisation of the specific-absorption, backscattering and scattering properties of phytoplankton and suspended particles along this coast is required to develop and test regional versions of the GIOP. In the subsequent analyses, we use OC3M and GSM to assess the spatial and temporal differences in these algorithms in coastal and shelf waters of the eastern Arabian Sea.

#### 4.3. Differences in Chla algorithms available for MODIS-Aqua along the eastern Arabian Sea coast

To date there have been few studies on the Chla dynamics of the eastern coast of the Arabian Sea. We therefore generated a Chla time-series from 2002–2011 and compared OC3M and GSM. In the north eastern coast, GSM consistently gave higher Chla compared to OC3M (Fig. 5). This region can be highly influenced by  $a_{CDOM}(\lambda)$ , which at certain times of the year accounts for 90% of the total light absorption (Menon et al., 2006). A combination of this and the errors in MODIS-Aqua  $R_{rs}(443)$  account for the differences observed between GSM and OC3M. In addition, if the  $S_{CDOM}$  and Chla specific-phytoplankton absorption coefficient ( $a_{ph}(\lambda)$ ) used in the GSM are too low, this would result in higher than expected Chla as observed along the north-east coast. In the central coastal area the difference between the algorithms was small (Fig. 5b). In the south eastern coast OC3M > GSM and *in situ*  $a_{CDOM}(\lambda)$  was low and the lower Chla may be attributed to the  $a_{CDOM}(\lambda)$  used in the parameterisation of the GSM compared to *in situ* values. On an operational basis in near shore coastal areas, GSM returned negative values because the inversion failed to find a realistic solution or because of negative  $R_{rs}(412)$  caused by atmospheric correction errors resulting in a significant number of pixel drop outs (Fig. 5). Further offshore, OC3M and GSM returned similar Chla values and there were no differences between the algorithms except in January 2005 (Fig. 6).

## 5. Conclusion

The eastern Arabian Sea coast in the north and south were principally Case 2 Chla-TSM-CDOM type, in contrast to the central eastern coast which was Case 2 TSM-CDOM type. Three MODIS-Aqua ocean colour algorithms were evaluated; OC3M was the most accurate, GSM showed a similar accuracy for the south eastern coast and GIOP was the least accurate. OC3M was more accurate because it principally used  $R_{rs}(488):R_{rs}(547)$  bands, which are less affected by errors in the atmospheric correction. The GSM and GIOP algorithms use  $R_{rs}(412)$  and  $R_{rs}(443)$  in the model inversion procedures. Atmospheric correction errors in these bands led to less accurate Chla estimates for GSM and GIOP. In addition, the error in GIOP Chla covaried with  $a_{CDOM}(\lambda)$ . A nine year Chla time series from 2002 to 2011 was generated for OC3M and GSM for three coastal regions of the eastern Arabian Sea. In the north-eastern coastal area influenced by river run-off and winter convection, GSM consistently gave higher Chla compared to OC3M. In the south-eastern coastal region affected by monsoon upwelling, OC3M consistently gave higher values than GSM which were closer to *in situ* Chla. In the central coastal region influenced both by convective mixing and monsoon upwelling, there was little difference between the two algorithms. This could imply that OC3 MODIS-Aqua is accurate in other optically complex coastal and shelf regions compared to semi-analytical algorithms.

## Acknowledgements

G. Tilstone was supported by the European Space Agency (ESA) Project COASTCOLOUR (Contract no. 22807/09/I-AM), A. Lotlikar

by a Partnership for Observation of the Global Oceans (POGO) Scientific Committee on Oceanic Research (SCOR) Visiting Fellowship to Plymouth Marine Laboratory, UK and P. Miller by Natural Environment Research Council (NERC) Oceans 2025 funding. *In situ* data were collected within the framework of the Satellite Coastal and Oceanographic Research (SATCORE) programme coordinated by the Indian National Centre for Ocean Information Services (INCOIS). All MODIS MLAC and GAC products were kindly provided by the NASA GES DAAC. NERC Earth Observation Data Archive and Analysis Service, UK (NEODAAS) provided computing facilities and data storage.

## References

- Antoine, D., d'Ortenzio, F., Hooker, S.B., Béchu, G., Gentili, B., Tailliez, D., Scott, A.J., 2008. Assessment of uncertainty in the ocean reflectance determined by three satellite ocean color sensors (MERIS, SeaWiFS and MODIS-A) at an offshore site in the Mediterranean Sea (BOUSSOLE project). *Journal of Geophysical Research* 113, C07013.
- Bailey, S.W., Werdell, P.J., 2006. A multi-sensor approach for the on-orbit validation of ocean color satellite data products. *Remote Sensing of Environment* 102, 12–23.
- Banse, K., English, D.C., 2000. Geographical differences in seasonality of CZCS-derived phytoplankton pigment in the Arabian Sea for 1978–1986. *Deep Sea Research Part II: Topical Studies in Oceanography* 47, 1623–1677.
- Banzon, V.F., Evans, R.E., Gordon, H.R., Chomko, R.M., 2004. SeaWiFS observations of the Arabian Sea southwest monsoon bloom for the year 2000. *Deep Sea Research Part II: Topical Studies in Oceanography* 51, 189–208.
- Bousquet, P., Caias, P., Miller, J.B., Dlugokencky, E.J., Hauglustaine, D.A., Prigent, C., Van der Werf, G.R., Peylin, P., Brunke, E.G., Carouge, C., Langenfelds, R.L., Lathiere, J., Papa, F., Ramonet, M., Schmidt, M., Steele, L.P., Tyler, S.C., White, J., 2006. Contribution of anthropogenic and natural sources to atmospheric methane variability. *Nature* 443, 439–443.
- Briand, A., Babin, M., Morel, A., Claustra, H., 1995. Variability in the chlorophyll-specific absorption-coefficients of natural phytoplankton—analysis and parameterization. *Journal of Geophysical Research—Oceans* 100, 13321–13332.
- Brock, J.C., McClain, C.R., Luther, M.E., Hay, W.W., 1991. The phytoplankton bloom in the northwestern Arabian Sea during the southwest monsoon of 1979. *Journal of Geophysical Research—Oceans* 96, 20623–20642.
- Campbell, J., Antoine, D., Armstrong, R., Arrigo, K., Balch, W., Barber, R., Behrenfeld, M., Bidigare, R., Bishop, J., Carr, M.-E., Esaias, W., Falkowski, P., Hoepffner, N., Iverson, R., Kiefer, D., Lohrenz, S., Marra, J., Morel, A., Ryan, J., Vedernikov, V., Waters, K., Yentsch, C., Yoder, J., 2002. Comparison of algorithms for estimating ocean primary production from surface chlorophyll, temperature, and irradiance. *Global Biogeochemical Cycles* 16, 1035.
- Chauhan, P., Mohan, M., Nayak, S., 2003. Comparative analysis of ocean color measurements of IRS-P4 OCM and SeaWiFS in the Arabian Sea. *IEEE Transactions on Geoscience and Remote Sensing* 41, 922–926.
- Chauhan, P., Mohan, M., Sarangi, R.K., Kumari, B., Nayak, S., Matondkar, S.G.P., 2002. Surface chlorophyll a estimation in the Arabian Sea using IRS-P4 Ocean Colour Monitor (OCM) satellite data. *International Journal of Remote Sensing* 23, 1663–1676.
- Darecki, M., Stramski, D., 2004. An evaluation of MODIS and SeaWiFS bio-optical algorithms in the Baltic Sea. *Remote Sensing of Environment* 89, 326–350.
- Desa, E., Suresh, T., Matondkar, S.G.P., Desa, E., 2001. Sea truth validation of SeaWiFS ocean colour sensor in the coastal waters of the Eastern Arabian Sea. *Current Science* 80, 854–860.
- Dierssen, H.M., 2010. Perspectives on empirical approaches for ocean color remote sensing of chlorophyll in a changing climate. *Proceedings of the National Academy of Sciences of the United States of America* 107, 17073–17078.
- Fargion, G.S., Mueller, J.L., 2000. Ocean Optics Protocols for Satellite Ocean Colour Sensor Validation, Revision 2. Greenbelt, Maryland, USA, NASA Goddard Space Flight Center, pp. 125–153.
- Franz, B.A., Werdell, P.J., 2010. A generalized framework for modeling of inherent optical properties in ocean remote sensing applications, In: *Proceedings of Ocean Optics*, Anchorage, Alaska, USA.
- Green, S.A., Blough, N.V., 1994. Optical-absorption and fluorescence properties of chromophoric dissolved organic-matter in natural waters. *Limnology and Oceanography* 39, 1903–1916.
- IOCCG, 2006. *Remote Sensing of Inherent Optical Properties: Fundamentals, Tests of Algorithms and Applications*. IOCCG, Dartmouth, Canada.
- Lee, Z.P., Carder, K.L., Arnone, R.A., 2002. Deriving inherent optical properties from water color: a multiband quasi-analytical algorithm for optically deep waters. *Applied Optics* 41, 5755–5772.
- Longhurst, 2007. *Ecological Geography of the Sea*, second edition. Academic Press.
- Madhupratap, M., Kumar, S.P., Bhattachari, P.M.A., Kumar, M.D., Raghukumar, S., Nair, K.K.C., Ramaiah, N., 1996. Mechanism of the biological response to winter cooling in the northeastern Arabian Sea. *Nature* 384, 549–552.
- Maritorena, S., Siegel, D.A., Peterson, A.R., 2002. Optimization of a semianalytical ocean color model for global-scale applications. *Applied Optics* 41, 2705–2714.

- Menon, H.B., Lotliker, A.A., Moorthy, K.K., Nayak, S.R., 2006. Variability of remote sensing reflectance and implications for optical remote sensing—a study along the eastern and northeastern waters of Arabian Sea. *Geophysical Research Letters* 33, L15602.
- Mohr, J.J., Forsberg, R., 2002. Remote sensing: searching for new islands in sea ice—coastlines concealed in polar seas are now more accessible to cartography. *Nature* 416, 3535.
- Morel, A., Maritorena, S., 2001. Bio-optical properties of oceanic waters: a reappraisal. *Journal of Geophysical Research C: Oceans* 106, 7163–7180.
- Mueller, J.L. et al., 2000. Above-water radiance and remote sensing reflectance measurements and analysis protocols, In: Fargion, G.S., Mueller, J.L. (Eds.), *Ocean Optics Protocols for Satellite Ocean Color Sensor Validation*. National Aeronautical and Space Administration, Washington, USA.
- O'Reilly, J.E., Maritorena, S., Mitchell, B.G., Siegel, D.A., Carder, K.L., Garver, S.A., Kahru, M., McClain, C., 1998. Ocean color chlorophyll algorithms for SeaWiFS. *Journal of Geophysical Research C: Oceans* 103, 24937–24953.
- O'Reilly, J.E., Maritorena, S., O'Brien, M.C., Siegel, D.A., Toole, D., Menzies, D., Smith, R.C., Mueller, J.L., Mitchell, B.G., Kahru, M., Chavez, F.P., Strutton, P., Cota, G.F., Hooker, S.B., McClain, C.R., Carder, K.L., Muller-Karger, F., Harding, L., Magnuson, A., Phinney, D., Moore, G.F., Aiken, J., Arrigo, K.R., Letelier, R., Culver, M., 2000. SeaWiFS Postlaunch Calibration and Validation Analyses, Part 3, vol. 11, NASA Technical Memorandum - SeaWiFS Postlaunch Technical Report Series, pp. 1–49.
- Petit, M., Gaspar, P., Lahet, F., Demagistri, L., Desruisseaux, M., Boschet, C., Rey-Valette, H., Lebras, J.-Y. 2003. SeAGeRH project: toward a service offisheries management assisted by satellites. In: *Proceedings of IEEE International Geoscience and Remote Sensing Symposium, IGARSS '03*, vol 7, p 4561–4563.
- Prieur, L., Sathyendranath, S., 1981. An Optical classification of coastal and oceanic waters based on the specific spectral absorption curves of phytoplankton pigments, dissolved organic-matter, and other particulate materials. *Limnology and Oceanography* 26, 671–689.
- Royer, F., Fromentin, J.M., Gaspar, P., 2004. Association between bluefin tuna schools and oceanic features in the western Mediterranean. *Marine Ecology-Progress Series* 269, 249–263.
- Sathyendranath, S., Cota, G., Stuart, V., Maass, H., Platt, T., 2001. Remote sensing of phytoplankton pigments: a comparison of empirical and theoretical approaches. *International Journal of Remote Sensing* 22, 249–273.
- Sathyendranath, S., Stuart, V., Irwin, B.D., Maass, H., Savidge, G., Gilpin, L., Platt, T., 1999. Seasonal variations in bio-optical properties of phytoplankton in the Arabian Sea. *Deep-Sea Research Part II-Topical Studies in Oceanography* 46, 633–653.
- Shanmugam, P., 2011. A new bio-optical algorithm for the remote sensing of algal blooms in complex ocean waters. *Journal of Geophysical Research—Oceans* 116, L15602.
- Shetye, S.R., Gouveia, A.D., Shenoi, S.S.C., 1994. Circulation and water masses of the Arabian Sea. *Proceedings of the Indian Academy of Sciences—Earth and Planetary Sciences* 103, 107–123.
- Strickland, J.D.H., Parsons, T.R., 1972. *A Practical Handbook of Seawater Analysis*. Fisheries Research Board of Canada, Canada.
- Tilstone, G.H., Angel-Benavides, I.M., Pradhan, Y., Shutler, J.D., Groom, S., Sathyendranath, S., 2011. An assessment of chlorophyll-a algorithms available for SeaWiFS in coastal and open areas of the Bay of Bengal and Arabian Sea. *Remote Sensing of Environment* 115, 2277–2291.
- Tilstone, G.H., Peters, S.W.M., van der Woerd, H.J., Eleveld, M.A., Ruddick, K., Schoenfeld, W., Krasemann, H., Martinez-Vicente, V., Blondeau-Patissier, D., Roettgers, R., Sorensen, K., Jorgensen, P.V., Shutler, J.D., 2012. Variability in specific-absorption properties and their use in a semi-analytical ocean colour algorithm for MERIS in North Sea and Western English Channel Coastal Waters. *Remote Sensing of Environment* 118, 320–338.
- Twardowski, M.S., Boss, E., Sullivan, J.M., Donaghay, P.L., 2004. Modeling the spectral shape of absorption by chromophoric dissolved organic matter. *Marine Chemistry* 89, 69–88.
- UNESCO, 1994. Protocols for Joint Global Ocean Carbon Flux Study (JGOFS) Core Measurements.
- Welschmeyer, N.A., 1994. Fluorometric analysis of chlorophyll a in the presence of chlorophyll b and pheophytins. *Limnology and Oceanography* 39, 1985–1992.
- Zibordi, G., Berthon, J.F., Melin, F., D'Alimonte, D., 2011. Cross-site consistent *in situ* measurements for satellite ocean color applications: the BiOMaP radiometric dataset. *Remote Sensing of Environment* 115, 2104–2115.
- Zibordi, G., Berthon, J.F., Melin, F., D'Alimonte, D., Kaitala, S., 2009. Validation of satellite ocean color primary products at optically complex coastal sites: Northern Adriatic Sea, Northern Baltic Proper and Gulf of Finland. *Remote Sensing of Environment* 113, 2574–2591.
- Zibordi, G., Melin, F., Berthon, J.F., 2006. Comparison of SeaWiFS, MODIS and MERIS radiometric products at a coastal site. *Geophysical Research Letters*, 33.